Materials & Design 254 (2025) 114088

Contents lists available at ScienceDirect

Materials & Design

journal homepage: www.elsevier.com/locate/matdes

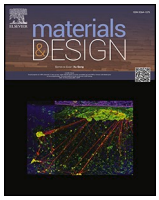

Metal fused filament fabrication (MF^3) of Ti-6Al-4 V implants by using flexible, partially water-soluble binder systems

Ralf Eickhoff [a,*], Steffen Antusch [a], Dorit Nötzel [a], Thomas Hanemann [a,b]

[a] Institute for Applied Materials, Karlsruhe Institute of Technology, Hermann-von-Helmholtz-Platz 1, D-76344 Eggenstein-Leopoldshafen, Germany
[b] Department of Microsystems Engineering, University Freiburg, Georges-Koehler-Allee 102, D-79110 Freiburg, Germany

ARTICLE INFO

Keywords:
Additive manufacturing
FFF
MEX
MF^3
Ti6Al4V
Water-soluble binder
Implants

ABSTRACT

Metal Fused Filament Fabrication provides a cost-efficient method to produce metal implants adapted to the patient. However, the limited flexibility of highly filled filaments and the reduced accuracy in comparison with alternative additive manufacturing techniques currently restrict the widespread implementation of this method. Building upon the findings of previous studies, the eco-friendly partially water-soluble binder systems containing polyethylene glycol (PEG), poly(vinylbutyral) (PVB) and poly(methylmethacrylat) (PMMA) were further optimized. Consequently, the influence of the plasticizer acetyltributylcitrate (ATBC) on the flow behavior and the flexibility of the filaments was investigated. The combination of all binder components, in conjunction with a solids content of 60 %, has enabled the fabrication of filaments with a high degree of usability, attributable to their remarkable flexibility and excellent printing properties. Following the debinding and sintering processes, the manufacturing of implants with densities that exceed 99.5 % of the theoretical values was feasible.

1. Introduction

Additive manufacturing (AM) was originally developed for the rapid production of models and prototypes. However, it has since established itself as a viable alternative in the manufacturing of critical components for the aerospace and automotive industries [1–4]. The medical field also offers significant potential, as every patient is unique, and thus, AM has considerable potential for use in personalized and customized medical applications [5]. While there are some reports about the fabrication of artificial tissues and organs [6–8], the primary focus is on the production of personalized implants made of polymers, metals, and ceramics. Examples of this include root analog implants [9], full-arch fixed dental prostheses [10] or crowns [11,12] in the field of dentistry, maxillofacial implants [13] or hip implants [14,15]. Furthermore, veterinary medicine is a field in which there is significant interest. Receiver-specific diagnosis and therapy are of particular importance in this discipline, due to the wide range of dimensions and anatomical variances that can be observed in animals [16,17].

Additive manufacturing of titanium and its alloys, a leading biomaterial, is of particular interest due to its challenging processing and low waste production, which is crucial given the high cost of the powder. The majority of the printed titanium implants are manufactured by means of powder bed fusion (PBF) methods, such as selective laser melting (SLM). This method is the most widely used due to the high level of geometric freedom and near net shape production [18]. However, the current limitations are high investment costs, safety measures and substantial energy consumption during printing. The latter can lead to changes in the microstructure and high anisotropy of the printed parts [19–21], as well as alterations of the microstructure and the morphology of the unused powder, which limits the recycling of the powder [22]. In order to reduce waste and enhance safety for both the environment and the operator, Metal Fused Filament Fabrication (MF^3) can be considered as a valid option [23]. In addition, it is possible to upgrade cost-effective commercial desktop Fused Filament Fabrication (FFF) printers in a simple and economical way to print metal-based parts [24,25]. As a result of these factors, the cost per unit is reduced compared to SLM [26]. Further advantages of this process include the homogeneous microstructure that results from the heat treatment, the wide range of materials that can be utilized [27], and the ability to combine different materials within the same object [28]. However, it should be noted that MF^3 is still in the early stages of development. The current challenges include the low flexibility of filled filaments, the poor level of detail, and

* Corresponding author.
E-mail addresses: ralf.eickhoff@kit.edu (R. Eickhoff), steffen.antusch@kit.edu (S. Antusch), dorit.noetzel@kit.edu (D. Nötzel), thomas.hanemann@kit.edu, thomas.hanemann@imtek.uni-freiburg.de (T. Hanemann).

https://doi.org/10.1016/j.matdes.2025.114088
Received 26 March 2025; Received in revised form 7 May 2025; Accepted 9 May 2025
Available online 10 May 2025

the inter-layer connectivity of the printed parts [29], as well as the low relative density of the final parts.

As with the similar powder injection molding, MF^3 is contingent upon following a process chain to avoid the aforementioned issues [30]. The process can be subdivided into five stages: (1) characterization, selection, and compounding of raw materials to the so-called feedstock; (2) extrusion of filaments; (3) printing of components using material extrusion (MEX); (4) debinding; and (5) heat treatment. An important step in the process is the selection of the polymers for the binder. Binder systems typically contain a range of polymers, the choice of which is determined by the rheological properties in conjunction with the metal powder, and the specific debinding method employed [27,31]. Special focus is also placed on compounding to ensure the homogeneity of the filaments and, consequently, the printed parts. Otherwise, there is a risk of filaments becoming inflexible and defects arising during subsequent steps [32,33].

There are three predominant debinding methods that are frequently utilized: thermal debinding, combined solvent and thermal debinding and catalytic debinding [34]. The most common way to remove the binder is thermal debinding, where parts are heated up until the polymeric binder degrades and diffuses out of the sample. While this method offers low requirements to the polymeric binder and includes only a few processing steps, it potentially leads to slow heating rates or defects in the samples. The combined solvent and thermal debinding addresses these issues. The solvent extraction of one polymer of the binder creates open pores, which reduce or prevent defects and enable higher heating rates in the subsequent thermal debinding. Solvent debinding is usually performed with organic solvents [35–37]. Nevertheless, there is an ongoing effort to substitute potentially hazardous organic solvents by water to reduce costs and the environmental impact [32]. A number of challenges remain, however, including the compatibility of the blended polymers to prevent binder separation and the extended debinding times for large components [38]. Catalytic debinding can be a convenient method of reducing the time required for extraction of the binder [39]. Nevertheless, this method is limited to only a few materials and polymers and requires specialized equipment to deal with the acid vapors that are responsible for the catalytic degradation [40]. The final step to obtain dense titanium parts is sintering, which is performed at temperatures of 70 to 90 % of the powder's melting point according to the Kelvin temperature scale. During this process, diffusion mechanisms lead to rearrangement, particle movement, and mass transport to reduce the surface energy by the formation of solid bonds between the powder particles. In addition, some of these diffusion processes also lead to a reduction in porosity, resulting in the shrinkage and densification of the parts. It is possible to adjust the microstructure by varying the sintering temperature and time, thus producing the desired material properties. In regard to the high affinity of titanium for oxygen, nitrogen, and carbon, and therefore to avoid the formation of oxides, nitrides, and carbides, sintering is performed in a vacuum or argon atmosphere. These contaminations result in an embrittlement of the produced parts. The standard ASTM F2885-17 provides a detailed description of the permissible level of contamination for medical implants manufactured using metal injection molding [41]. However, research has indicated that a marginally elevated oxygen content can enhance the mechanical properties without compromising the elongation [42].

2. Materials and methods

2.1. Material selection

2.1.1. Titanium powder

Due to their high mechanical load and the demanded durability, medical implants have high requirements in order to avoid subsequent surgical interventions. An important factor is the carbon and oxygen content, which is described in the standard ASTM F2885-17 [41] for surgical Ti-6Al-4 V implants made by powder injection molding. Due to the similiarity of the feedstock compositions of MF^3 and metal injection molding, the requirments can be derived from this standard. Both elements lead to enbrittlement of the implant and thus lower the demanded elongation. As contamination from the process chain cannot be ruled out, a Ti-6Al-4 V alloy powder with medical grade was selected (Grade 23, Tekna Advanced Materials Inc., Sherbrooke, Canada), which is characterized by its low carbon (0.007 wt%) and oxygen content (0.086 wt%). In order to adapt the polymeric binder to the selected powder, the particle density by Helium pycnometry (AccuPyc II 1340, Micromeritics Instr. Corp., Norcross, GA, USA), the specific surface area (SSA) via the BET method (Gemini VII 2390, Micromeritics Instr. Corp., Norcross, GA, USA) and the particle size distribution by laser diffraction (LA-950 Horiba Ltd., Kyoto, Japan) were measured. The knowlegde about these properties is important to predict the rheological properties of the later feedstocks. Table 1 gives an overview of the measured particle properties.

2.1.2. Thermoplastic binder system

The thermoplastic binder fulfills a number of functions. The binder has to ensure a homogeneous distribution of the powder and a low viscosity of the feedstocks. Additionally, it must provide sufficient flexibility to the filaments, enabling them to be wound onto and from spools, thereby ensuring their usability. Furthermore, it keeps the powder particles in their shaped form until the sintering phase. It must also be possible to remove the binder properly and without leaving any residue. In order to fulfill all of the aforementioned requirements, the binder consists of at least three components. The high-viscosity backbone polymers poly(vinyl butyral) (PVB Mowital 30H, Kuraray Europe GmbH, Frankfurt, Germany) and poly(methyl methacrylate) (PMMA Degalan G7E, Roehm GmbH, Darmstadt, Germany) provide strength of the filaments and during the first debinding step in water. The low molecular weight and water-soluble base polymer polyethylene glycol (PEG 8,000 and PEG 20,000, C. Roth GmbH Co. KG, Karlsruhe, Germany) ensures low viscosity of the feedstocks and defect-free debinding. The additive acetyltributyl citrate (ATBC, Sigma Aldrich, St. Louis, USA) is a common substitute for phthalates and acts as a plasticizer, ensuring sufficient flexibility of the filaments. In addition to the manufacturer's specifications, the density and the thermal behavior of the organic components were characterized by Helium pycnometry (AccuPyc II 1340, Micromeritics Instr. Corp., Norcross, GA, USA) as well as Thermogravimetric Analysis (TGA) and Differential Scanning Calorimetry (DSC) measurements (Netzsch STA 449 F3 Jupiter, Netzsch GmbH & Co. KG, Selb, Germany). The measured properties are displayed in Table 2. The softening and decomposition temperatures were derived from the TGA-DSC measurements.

2.1.3. Feedstock compositions

The present study examined three distinct binder compositions: The compositions under investigation were PVB/PEG, PMMA/PEG, and PMMA/PVB/PEG (Table 3). For all feedstocks, ATBC was selected as the additive to ensure sufficient flexibility of the later filaments. In the case of the PVB/PEG composition, PEG 20,000 was employed to forestall the separation of the binder, which was observed in previous research [43]. In order to prevent a significant increase in viscosity, the low molecular weight base polymer PEG 8,000 was utilized in combination with the high molecular weight PMMA. Due to possible inhomogeneities caused by the size of the cylindrical PMMA G7E pellets (2.5 mm x 3.0 mm), smaller PMMA granules (0.5 mm x 3 mm) were produced by extrusion with a capillary rheometer at 210 °C and subsequent pelletization with

Table 1
Particle properties.

Ti-6Al-4 V	Density (g/cm^3)	D_{10} (µm)	D_{50} (µm)	D_{90} (µm)	SSA (m^2/g)
Measured	4.4	13.2	28.6	47.3	0.15

Table 2
Properties of the binder components used (T_S: softening temperature, T_D: decomposition temperature).

Component	Density (g/cm^3)	M_W (g/mol)	T_S (°C)	T_D (°C)
PMMA G7E	1.18	159,000[V]	106	252
PVB 30H	1.11	32,000–35,000[V]	64	286
PEG 8,000	1.22	7,300–9,000[V]	66	343
PEG 20,000	1.22	20,000[V]	69	372
ATBC	1.05	402[V]	−80[V]	226

V: Vendor's data sheet.

Table 3
Overview of the binder compositions investigated.

Combination	PVB 30H (vol. %)	PMMA G7E (vol.%)	PMMA kG7E (vol.%)	PEG 8,000 (vol. %)	PEG 20,000 (vol.%)	ATBC (vol. %)
PVB 50/ PEG 48.6/ ATBC 1.4	50	–	–	–	48.6	1.4
PVB 50/ PEG 47.2/ ATBC 2.8	50	–	–	–	47.2	2.8
PVB 50/ PEG 44.3/ ATBC 5.7	50	–	–	–	44.3	5.7
PMMA 40/ PEG 54.3/ ATBC 5.7	–	40	–	54.3	–	5.7
PMMA 40/ PEG 51.4/ ATBC 8.6	–	40	–	51.4	–	8.6
PMMA 40/ PEG 48.7/ ATBC 11.3	–	40	–	48.7	–	11.3
PMMA 40/ PEG 45.9/ ATBC 14.1	–	40	–	45.9	–	14.1
PMMA 40/ PEG 54.3/ ATBC 5.7 (kG7E)	–	–	40	54.3	–	5.7
PMMA 40/ PEG 51.4/ ATBC 8.6 (kG7E)	–	–	40	51.4	–	8.6
PMMA 40/ PEG 48.7/ ATBC 11.3 (kG7E)	–	–	40	48.7	–	11.3
PMMA 40/ PEG 45.9/ ATBC 14.1 (kG7E)	–	–	40	45.9	–	14.1
PMMA 25/ PVB 25/ PEG 44.3/ ATBC 5.7	25	25	–	44.3	–	5.7
PMMA 25/ PVB 25/ PEG 44.3/ ATBC 5.7 (kG7E)	25	–	25	44.3	–	5.7
PMMA 22.5/ PVB 22.5/ PEG 49.3/ ATBC 5.7 (kG7E)	22.5	–	22.5	49.3	–	5.7
PMMA 20/ PVB 20/ PEG 54.3/ ATBC 5.7 (kG7E)	20	–	20	54.3	–	5.7

an impact mill. The use of the smaller PMMA pellets, designated as PMMA kG7E, is indicated in the appropriate sections. The additive concentration was calculated as a percentage by weight of the total binder and subtracted from the base polymer PEG. To achieve the desired densities of the manufactured parts after sintering, it is essential to use titanium powder feedstocks with a high solid content. However, a high solid loading increases the viscosity of the feedstocks and can reduce the flexibility of the filaments. Accordingly, a solid load of 60 vol % was selected for all feedstock systems in order to reconcile both objectives.

2.2. Compounding and extrusion

A torque recording mixer-kneader (W50-EHT, Brabender GmbH, Duisburg, Germany) was used for the compounding of the feedstocks. The applied parameters can be found in Table 4. Due to the different glass transition temperatures of the two backbone polymers, the compounding temperatures were set to 125 °C (PVB), 160 °C (PMMA/PVB) and 170 °C (PMMA). To ensure comparable compounding behavior, the loading of the mixer was always the same: first, a small amount of titanium powder was fed into the mixing chamber. Subsequently, the backbone polymer and the base polymer were added. Then the ATBC was poured into the chamber and finally the rest of the metal powder was added successively. In order to investigate the inhomogeneities generated by the use of PMMA, as referenced in the previous section, the blade's rotating speed was set to 30 and 60 rpm, and the mixing time to 1, 1.5, 2, and 3 h. As outlined in [44] for this kneader, this set-up is equivalent to a shear rate of 2 to 36 1/s and 4 to 72 1/s. Each system was compounded once. For statistical purposes, three different feedstock systems were measured three times. The results are shown in the supplementary material (S 1a-c). Following the compounding process, the molding compounds were pelletized using an impact mill (Granulator 1514, Rapid Germany, Kleinostheim, Germany). The granulates produced were then shaped into filaments by a single screw filament extruder (Noztek pro HT, Noztek, Shoreham, UK). The desired filament diameter was 2.85 mm instead of the widespread 1.75 mm. Due to the larger diameter in relation to the volume of the fed material, this reacts less sensitively to diameter fluctuations, which leads to smaller fluctuations in the volume of the extruded feedstock. The extruder's accuracy, when operated with the same parameters, has a margin of error of ± 0.05 mm. To account for the swelling of the feedstocks, different nozzle diameters were used to achieve the desired filament diameter of 2.85 mm. Minor deviations from the target filament diameter can be addressed during the printing step using the slicer software. The extrusion parameters used for the different feedstocks can be found in the respective sections. The filaments were cooled by using a fan and then wound onto a spool by using a winder (Noztek Filament Winder 1.0, Noztek, Shoreham, UK). If the filaments did not demonstrate sufficient flexibility, they were extruded onto a metal cooling track and cut off at 50 cm.

2.3. Rheological characterization

The shear dependent viscosity was investigated by a high-pressure capillary rheometer (Rheograph 25, Göttfert Werkstoff-Prüfmaschinen GmbH, Buchen, Germany). The Weissenberg-Rabinowitsch correction was applied to enhance the precision of the measured values. To

Table 4
Overview of the compounding parameters used.

Combination	Temperature (°C)	Rotating speed (rpm)	Time (h)
PVB/PEG	125	30	2
PMMA/PEG	170	30, 60	2
PMMA/PVB/PEG	160	30, 60	1, 1.5, 2, 3

compare the produced feedstocks, the same parameters were used for all feedstocks, which are listed below.

- Temperature: 160 °C,
- Capillary length and diameter: 30 and 1 mm,
- Shear rate range: 1 to 3000 1/s.

In addition, and in continuation of a method introduced in previous work to quantify the flexibility of the filaments [32], the temperature dependent viscoelastic behavior was characterized by oscillatory measurements in the temperature sweep (TS) mode by a dynamic mechanical analyzer (DMA 242 E Artemis, Netzsch GmbH & Co. KG, Selb, Germany) equipped with a dual cantilever sample holder (2 x 16 mm free bending length). Therefore, the same parameters were applied. The samples used were filament pieces measuring 50 mm in length.

- Temperature: 20–50 °C,
- Frequency: 0.5 Hz,
- Amplitude: 50 μm,
- Pre-force: 0.1 N.

Each system was analyzed once. Three different feedstock systems were measured three times for statistical purposes. The results are shown in S 2a-c and S 3a-c.

2.4. Fused filament fabrication

A commercial but slightly modified FFF printer (x350pro, German RepRap, Feldkirchen, Germany) was used for printing. The printhead is depicted in Fig. 1. The original extruder was replaced by a Bondtech QR Extruder (Värnamo, Sweden) with Dual-Drive technology and an E3D V6 Hotend for 2.85 mm filaments (Oxfordshire, UK). This type of extruder offers higher precision and the printing of softer filaments. Part surface ventilation was installed for a higher level of detail of the printed parts. Furthermore, the print bed was covered with spring steel coated with PE tape to enhance adhesion and improve the removal of printed parts. Ultimaker Cura (V 5.4.0) was used for slicing. For subsequent characterization such as debinding behavior and density, ten cubic specimens (10 mm x 10 mm x 2.5 mm) were printed. A sketch can be found in [25]. The printing parameters are listed in Table 5. The infill density of 105 % was selected to prevent the formation of characteristic voids during the printing process. Feedstock-specific parameters such as the temperature as well as deviations from Table 5 can be found in the respective sections.

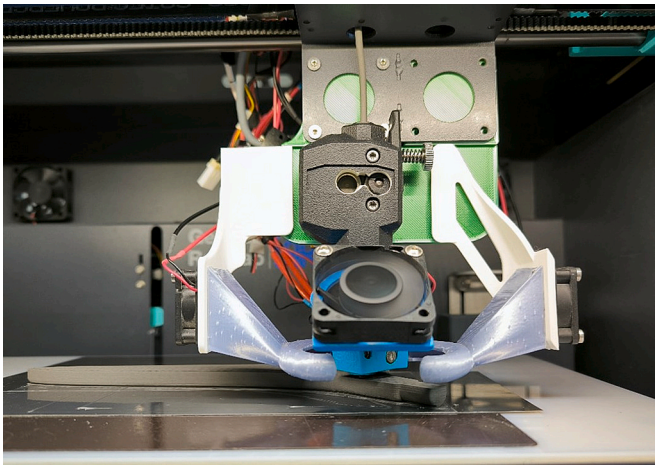

Fig. 1. Modified FFF printer x350 pro.

Table 5
Overview of the printing parameters used.

Parameter	Value	Parameter	Value
Infill density	105 %	Layer height	0.1 mm
Infill angle offset	90°	Nozzle size	0.4 mm
Infill pattern	Rectilinear	Number of walls	2
Infill overlap	0.2 mm	Printing speed	8 mm/s

2.5. Debinding and sintering

Debinding was carried out in a two-step process: first, PEG was removed in water for 24 h and at 30 °C, which creates open pores. This step reduces the thermal debinding time and prevents debinding-related defects such as blisters and cracks. Afterwards, the parts were dried overnight in a vacuum drying furnace (Vacutherm VT 6130P, Heraeus, Hanau, Germany) at 40 °C to remove residual water. Then, thermal debinding was carried out prior to sintering in a metal sinter furnace (MUT Advanced Heating GmbH, Jena, Germany). Two different thermal debinding strategies were investigated, which are depicted in Table 6. Strategy 1 aims to prevent defects and contamination during the debinding process. Strategy 2 is a cost-effective approach that effectively examines the potential of a binder system, but increases the risk of contamination with oxygen. The samples were then sintered with a heating rate of 5 °C/min, a maximum temperature of 1350 °C, and a sintering time of 4 h. In order to avoid contamination from oxygen and nitrogen, both thermal debinding and sintering were conducted under argon atmosphere (purity > 99.999 vol%, ALPHAGAZ 1 Argon, Air Liquide, Düsseldorf, Germany) in the same furnace.

2.6. Characterization of sintered samples

Density measurements of the printed and sintered samples were carried out using the Archimedes principle (Secura 225D-1S equipped with YDK 01, Sartorius Lab Instruments GmbH & Co. KG, Göttingen, Germany). The pycnometer density of the Ti-6Al-4 V powder was used as a basis for relative density calculations. A combustion analysis (CS600 and TC600, LECO 176 Instruments GmbH, Mönchengladbach, Germany) was carried out to characterize the final carbon and oxygen content in the sintered parts. CT images for defect analysis were conducted on a GE phoenix v|tome|x s240 (General Electric, Boston, MA, USA).

3. Results and discussion

3.1. PVB/PEG

PVB/PEG binder systems are widely used in powder injection molding and FFF, especially in combination with ceramic powders [45–47]. PVB is known for its good combustion without leaving any residue, as well as its excellent compatibility with other polar polymers, such as PEG [43]. In addition, there are many different types of plasticizers that are widely used for PVB, including the sustainable and non-hazardous ATBC [48]. In this work, three different ATBC contents and their influence on the rheological and processing properties were

Table 6
Thermal debinding strategies.

Strategy	Heating rate(K/min)	Temperature (°C)	Dwell time (h)	Specialty
1	0.5	550	1	Additional dwell time of 1 h at 300 and 400 °C
2	1.5	550	1	Pre-debinding at 250 °C for 4 h in air with a heating rate of 0.2 K/min

investigated.

3.1.1. Compounding and extrusion

The influence of the ATBC content on the torque curves is depicted in Fig. 2. The overall compounding behavior aligns with the theoretical curve, which can be divided into three phases: the filling phase, the mixing phase, and the equilibrium phase [49]. However, there is a substantial decrease in the torque between 15- and 40-min. Pre-studies have indicated that this is the point when the ATBC is integrated between the polymer chains. The curves also show no significant differences between the three ATBC contents, which is likely due to the low concentrations used.

The feedstocks were then extruded into filaments at a temperature of 70 °C and a nozzle diameter of 2.7 mm. All filaments demonstrated the necessary flexibility to be wound onto a spool.

3.1.2. Rheological characterization

As already indicated by the torque curves during compounding, the viscosity of the three feedstocks is very similar (Fig. 3a). According to the literature, the range of the shear rate for FFF is between 40 and 450 s^{-1} [32,50,51], depending on the utilized binder system and the printing parameters, such as nozzle size, layer height or printing speed [52]. Within this range, all three feedstocks remain below 1000 Pas, which is a reliable indicator for determining the feasibility of processing the feedstock. However, a slight difference is evident in the flexibility of the filaments. Previous work has indicated that a storage modulus of less than 600 MPa at 25 °C is an effective benchmark for assessing filament flexibility [32]. As illustrated in Fig. 3b, even very small ATBC concentrations provide excellent flexibility. This phenomenon can be attributed to the interaction between the ATBC molecules and the PVB chains, where the ATBC molecules bond to the dipoles of polymer chains and disrupt the strong hydrogen bonds.

3.1.3. Fused filament fabrication

As shown in the two previous sections, all of the filaments possessed sufficient flexibility to be wound onto a spool, thereby exhibiting excellent usability. However, the filament containing 5.7 vol% ATBC showed a very high degree of flexibility and softness, which complicated the extrusion. In addition, the low viscosity and the slow solidification also limited the printing of complex geometries with overhangs. Despite the implementation of strong part ventilation, the samples continued to collapse. Conversely, the feedstocks with reduced ATBC content exhibited a distinct behavior. The rapid solidification of these feedstocks enabled the printing of complex geometries. Nevertheless, the low viscosity of all three materials enabled their printing at an extrusion temperature of 160 °C and a bed temperature of 40 °C.

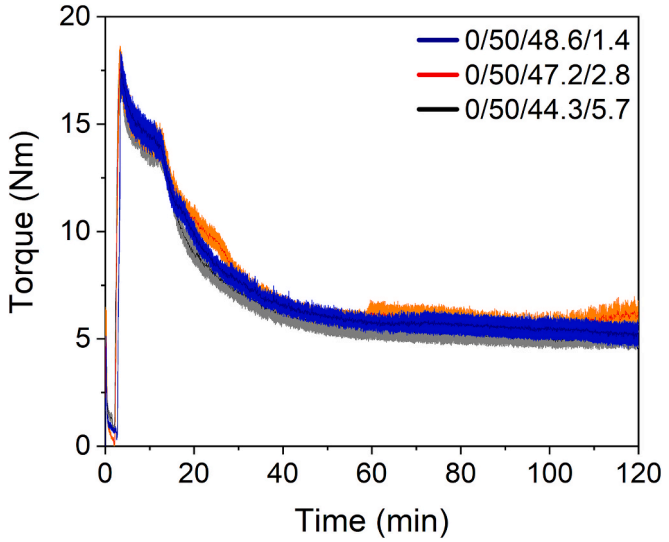

Fig. 2. Compounding of PVB/PEG based binder (125 °C) with different ATBC content (PMMA/PVB/PEG/ATBC).

3.1.4. Debinding and sintering

Debinding was carried out in a two-step process: First, the PEG was removed in water at 30 °C. Fig. 4a shows the pore fraction, calculated from the mass loss after solvent debinding, in the samples after 24 h. It can clearly be seen that a higher ATBC content led to a smaller pore fraction. There are two reasons for this observation. On the one hand, the substitution of PEG with ATBC leads to a reduction in PEG content and, consequently, a decrease in the water-soluble fraction of the binder. On the other hand, the non-water-soluble polymers act as a barrier, thereby enhancing this effect as the amount increases. Nevertheless, according to literature, the pore fraction is sufficient enough for a defect-free thermal debinding [38]. Challenging is the low green body strength during debinding in water, which is due to the high water absorption of PVB [53]. The volume of the samples increases approximately two-fold in water, but this increase in volume is reversible. Despite the significant change in sample volume, no defects were found in the final components after sintering (see S 4a-b). However, parts with complex or large geometries exhibited persistent deformations. Furthermore, no characteristic pores from the printing process, which were observed in [54], were found in the samples.

In contrast to the fatty acids examined in previous studies [32,43], feedstocks containing ATBC present significant challenges when it comes to thermally debinding without defects (Fig. 4b). While parts with 5.7 vol% fatty acid were debinded with a fast heating rate of 1.5 K/min without showing any visible defects, the same amount of ATBC resulted in a lot of small blisters within the samples even at a slow heating rate of 0.5 K/min (strategy 1). This is likely attributable to the strong bonding of the ATBC molecules to the PVB chains. However, a pre-debinding process at 250 °C in air (strategy 2) prevents the formation of blisters due to the low decomposition temperature of ATBC (226 °C). In this case, the majority of ATBC is eliminated, which subsequently reduces the potential for issues during the actual debinding step. With lower ATBC contents (1.4 vol% and 2.8 vol%), no problems occurred during thermal debinding. Both strategies showed comparable relative densities, with strategy 1 exhibiting slightly higher values. The best relative densities of approximately 98 % were observed for the feedstocks with 1.4 vol% ATBC.

3.2. PMMA/PEG

In contrast to PVB/PEG binder systems, PMMA/PEG is more frequently utilized in metal injection molding than in ceramic injection molding [55,56]. This discrepancy can be attributed to the comparatively higher molecular weight of PMMA in comparison to PVB, which results in an elevated viscosity of the feedstocks. Therefore, this binder system is usually only compatible with the coarser metal powders that possess good flow properties. Due to the high molecular weight of the used PMMA and to reduce the viscosity of the feedstocks, higher proportions of PEG and a lower molecular weight PEG (PEG 8,000) were used in comparison to the PVB-based feedstocks.

3.2.1. Compounding and extrusion

In contrast to the torque curves of PVB/PEG, the PMMA/PEG curves deviate from the theoretical mixing curves. As illustrated in Fig. 5a, the compounding behavior of four feedstocks with different ATBC contents at 30 rpm is shown. There were no significant differences observed. However, the torque increases significantly between 40 and 70 min. This is due to the liquefaction and the integration of the relatively large PMMA granules, which have an approximate size of 3 mm, into the feedstock. Nevertheless, this increase is still relatively low compared to the torque curves of PVB/PEG and within a range of 4 Nm. To ensure a

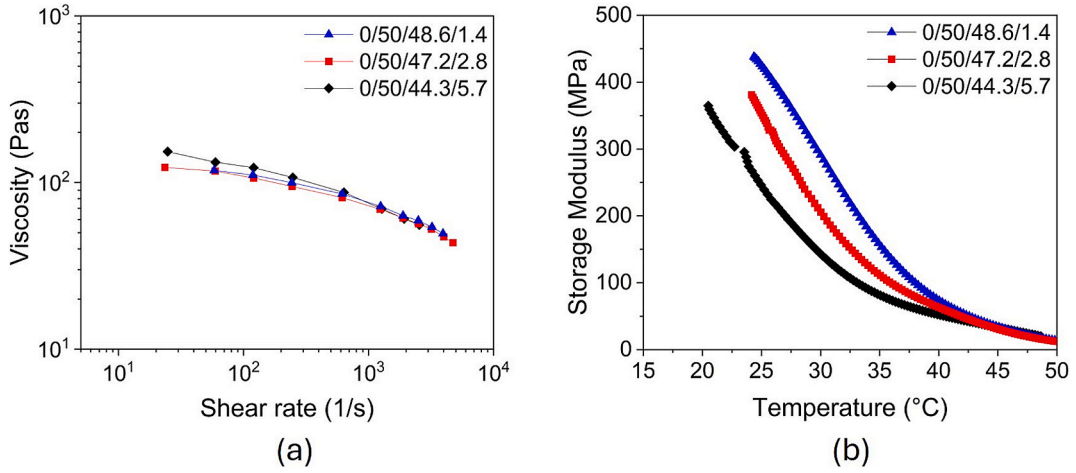

Fig. 3. (a) Capillary rheology at 160 °C and (b) temperature sweeps of PVB/PEG based feedstocks with different ATBC content (PMMA/PVB/PEG/ATBC).

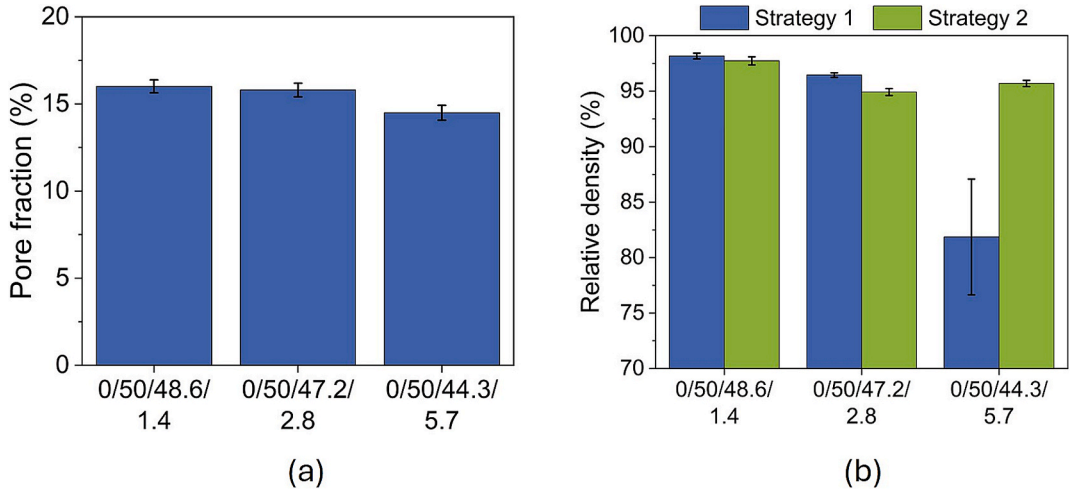

Fig. 4. (a) Pore fraction in samples with different ATBC content after 24 h at 30 °C and (b) relative density of the samples depending on the used thermal debinding and sintering program (PMMA/PVB/PEG/ATBC).

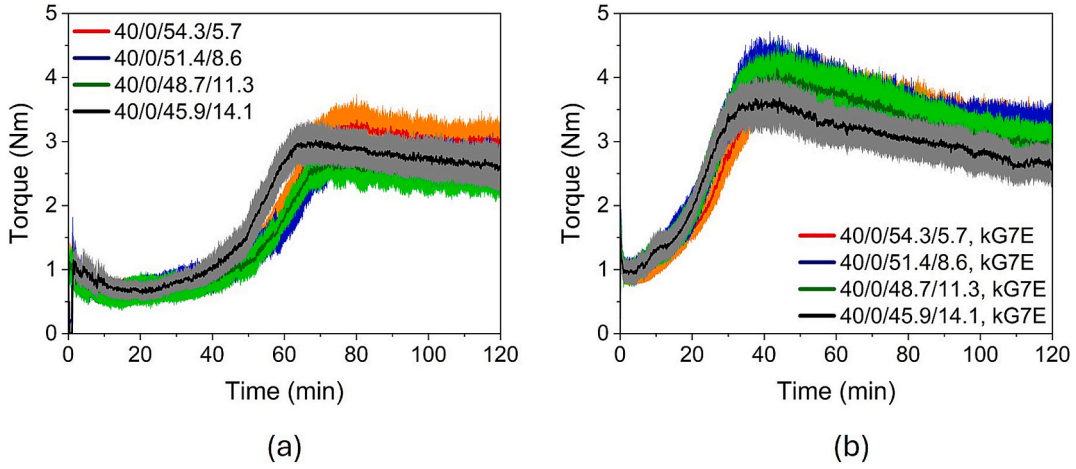

Fig. 5. Compounding of PMMA/PEG based binder (170 °C) with different mixing parameters; (a) Variation of ATBC content at 30 rpm and (b) variation of ATBC content at 60 rpm and PMMA kG7E (PMMA/PVB/PEG/ATBC).

higher level of homogeneity, the four different compositions were also produced with the smaller PMMA granules (kG7E) and a higher blade speed of 60 rpm (Fig. 5b). This led to earlier liquefaction and the integration of the PMMA pellets into the feedstocks with a slightly lower increase in torque. However, no observable difference in torque was identified at the end of the compounding process when comparing these

two distinct production methods. The feedstocks were then extruded into filaments at temperatures of 60 to 70 °C using a nozzle size of 2.7 mm for the stiff filaments and 2.95 mm for the flexible filaments. However, the nozzle size is process-related and not material-related. Only the filament produced with 14.1 vol% ATBC, smaller PMMA pellets and a blade's rotational speed of 60 rpm showed sufficient flexibility to be wound onto a spool.

3.2.2. Rheological characterization

3.2.2.1. Capillary rheology. The impact of the ATBC content on the viscosity of the feedstocks was found to be negligible. No notable differences were observed in the viscosity of the feedstocks manufactured with commercial PMMA G7E (Fig. 6a) granules or those produced with smaller PMMA pellets (Fig. 6b) at a higher shear rate. However, the latter led to a slight decrease in viscosity of approximately 100 to 200 Pas, which is probably the result of thermomechanical degradation and thus the reduction of the molecular weight of PMMA. Paci et al. observed a similar trend in PET [57]. In addition, the enhanced integration of the shorter PEG and ATBC molecules between the PMMA chains amplifies their lubricating properties. Nevertheless, the viscosity of all eight feedstocks remained below 1000 Pas in the shear range for FFF.

3.2.2.2. DMA. In contrast to the shear viscosity, the ATBC content showed a significant influence on the flexibility of the filaments. It was observed that an increase in additive content resulted in an enhancement of filament flexibility. However, all filaments produced with the commercial PMMA G7E pellets and a blade rotational speed of 30 rpm exhibited brittle behavior. As illustrated in Fig. 6c, the storage modulus for all filaments consistently exceeds 600 MPa at 25 °C. On the contrary, the smaller PMMA granulates and the higher shear rate during compounding resulted in a lower storage modulus, especially for the feedstocks with a high ATBC content (Fig. 6d). However, only the filament containing 14.1 vol% additive showed values below 600 MPa at 25 °C. It is noteworthy that, in comparison to PVB, a significantly higher additive concentration is required to achieve plasticization of PMMA. This is probably due to the weaker bonding of ATBC to PMMA compared to PVB. For this reason, and because of the high processing temperature of PMMA, ATBC is not a common plasticizer for PMMA. Consequently, no literature could be found.

3.2.3. Fused filament fabrication

In contrast to the PVB-based feedstocks, as outlined in the previous section, only one filament was sufficiently flexible to be wound onto a spool. The rest of the filaments had to be fed into the extruder one by one in pieces of 50 cm each one after the another. All filaments showed excellent mechanical stability, ensuring no extrusion issues occurred. Due to the comparable shear viscosity, an extrusion temperature of 170 °C and a bed temperature of 40 °C was suitable for all materials. The

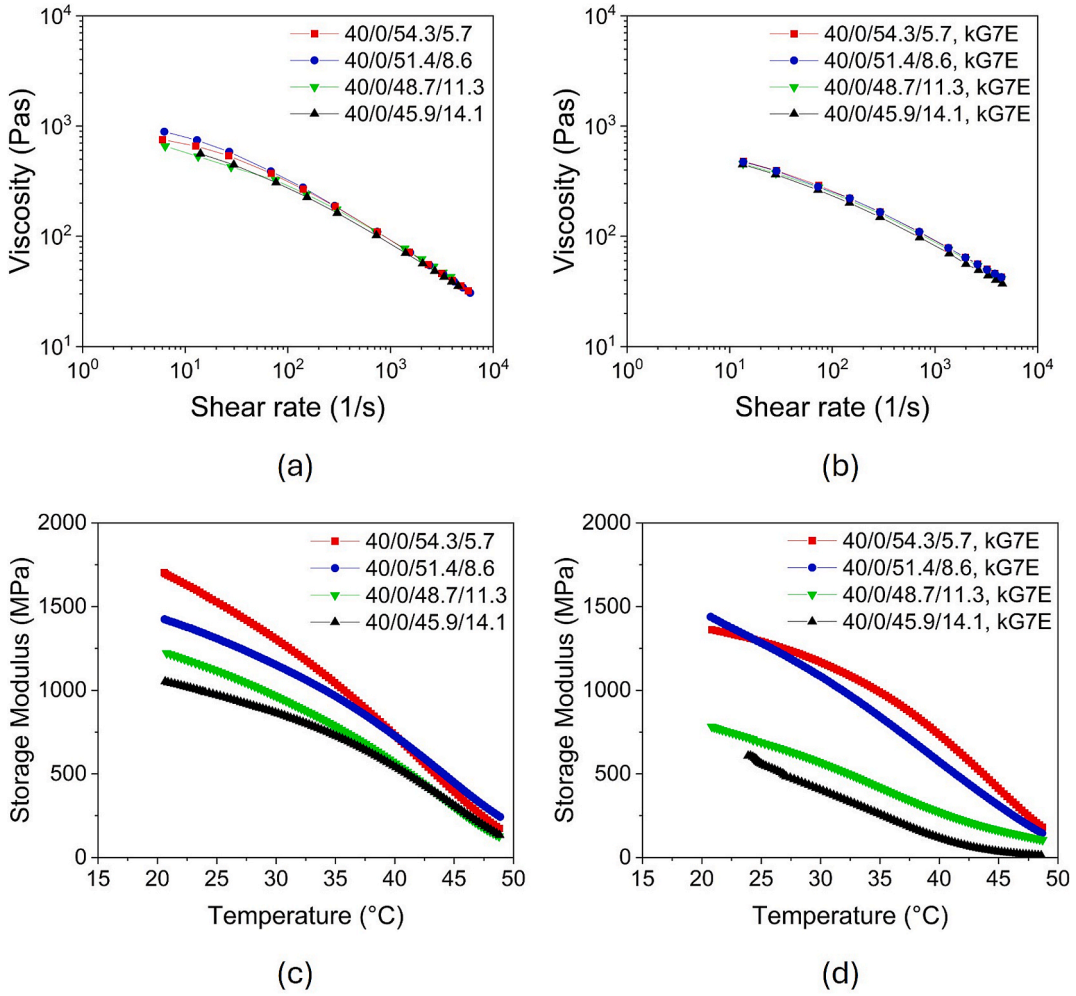

Fig. 6. Capillary rheology of PMMA/PEG based feedstocks at 160 °C with different mixing parameters; (a) Variation of ATBC content at 30 rpm and (b) variation of ATBC content at 60 rpm and PMMA kG7E. Temperature sweeps of PMMA/PEG based feedstocks with different mixing parameters; (c) Variation of ATBC content at 30 rpm and (d) variation of ATBC content at 60 rpm and PMMA kG7E (PMMA/PVB/PEG/ATBC).

windable filament demonstrated exceptional printing properties, enabling the printing of large components such as the stem of a hip implant (Fig. 7a) with a nozzle diameter of 0.8 mm and small components like dental implants (Fig. 7b) with a nozzle size of 0.15 mm. However, a current challenge is the slow solidification of the parts during printing. Despite the implementation of strong part cooling, printing large overhangs remains challenging.

3.2.4. Debinding and sintering

Due to the high PEG contents, the samples showed a high pore fraction between 16 and 20 % after debinding 24 h in water (Fig. 8a). As expected, the number of pores decreased with increasing ATBC content. The reasons behind this observation are similar to the PVB-based feedstocks, including the decreasing PEG content in the samples and the barrier effect of the non-water-soluble polymers. There is a slight distinction between the two feedstock production methods, which becomes more prominent with increasing ATBC concentration. This behavior is probably due to the elevated thermomechanical degradation of the PMMA chains during the compounding process at higher shear rates. This results in a lower molecular weight, which consequently leads to reduced entanglement between the polymer chains. This effect becomes more significant as the ATBC content increases. In contrast to PVB, PMMA possesses excellent water resistance, thereby preventing any deformations.

Similar to the PVB-based feedstocks, issues occurred again through the addition of ATBC regarding thermal debinding. Fig. 8b illustrates the relative densities of the samples as a function of ATBC content and debinding strategy. Strategy 1 demonstrated significant inconsistency in density across the ATBC content range. This is likely attributable to the inhomogeneous formation and size of the observed blisters. The highest values were observed at 8.6 vol% and 11.3 vol% ATBC. Small blisters were only observed in a few samples. In contrast, the pre-debinding of strategy 2 resulted in very similar densities of approximately 94–95 %, regardless of the production method. However, it should be noted that, in general, all measured densities were quite low compared to the densities of the PVB-based feedstocks. Therefore, no sample meets the standard of 96 % [41]. This finding aligns with the results of previous studies [32,43] and the values derived from metal injection molding with a similar powder loading as reported in literature [58]. However, higher solid contents and slight modifications of the binder systems resulted in densities of approximately 98 % [59,60].

3.3. PMMA/PVB/PEG

Despite of the unique advantages and disadvantages of the binder combinations PVB/PEG and PMMA/PEG, there is only one report about blending these two polymers to utilize the strengths of both binder systems [32]. Preliminary tests have shown that 5.7 vol% ATBC, in combination with PVB, PMMA, and PEG 8000 provides sufficient flexibility. Furthermore, as previously indicated, ATBC can cause problems during thermal debinding. Therefore, the amount of ATBC should not exceed this content and amount of 5.7 vol% for all binder systems investigated.

3.3.1. Compounding and extrusion

In this study, the ratio of PMMA to PVB was maintained at an equal level, with a precise proportion of one to one. Therefore, the influence of the commercial PMMA G7E and the smaller PMMA kG7E as well as the compounding parameters such as mixing time and blade's rotational speed on the feedstock properties was examined. In addition, investigations were conducted into higher than 44.3 vol% PEG content. Higher PEG content offers advantages, such as faster solvent debinding times and potentially faster heating rates during thermal debinding in the subsequent debinding step. However, as described in [32], it can also reduce the flexibility of the filaments. Table 7 gives an overview of all examined feedstock compositions and compounding parameters.

Fig. 9a shows the impact of the utilized PMMA and blade's rotational speed. As anticipated, the integration of the PMMA pellets is accelerated by the use of smaller PMMA granules and a higher shear rate. In particular, the combination of both led to a significant increase in torque. Despite this, all three feedstocks exhibited similar torque values at the end of the compounding process. Furthermore, the torque curve reaches equilibrium after approximately 120 to 140 min, which is significantly later than with the pure PVB and PMMA feedstocks (Fig. 9b). The influence of an increasing PEG content on the compounding behavior is depicted in Fig. 9c. Generally, a higher PEG content resulted in a lower torque, which can be attributed to the lower molecular weight of the utilized PEG 8,000 compared to PMMA. This results in a reduced entanglement between the polymer chains, leading to a lower viscosity. However, the torque curves continued to rise until the end of the compounding process, indicating an inhomogeneous feedstock, where the PMMA pellets have not yet fully integrated. An increase in the shear rate led to faster integration of the PMMA pellets into the feedstocks, resulting in a significant increase in torque. Due to the lower PMMA content, the increase was more modest with a higher PEG content. At the end of the compounding process, the torque curves of each composition converge. Furthermore, it was observed for the feedstock with 54.3 vol% PEG and a blade's rotational speed of 60 rpm that a liquid phase separated from the feedstock during the compounding process and was expelled from the mixing chamber (see S 5a-

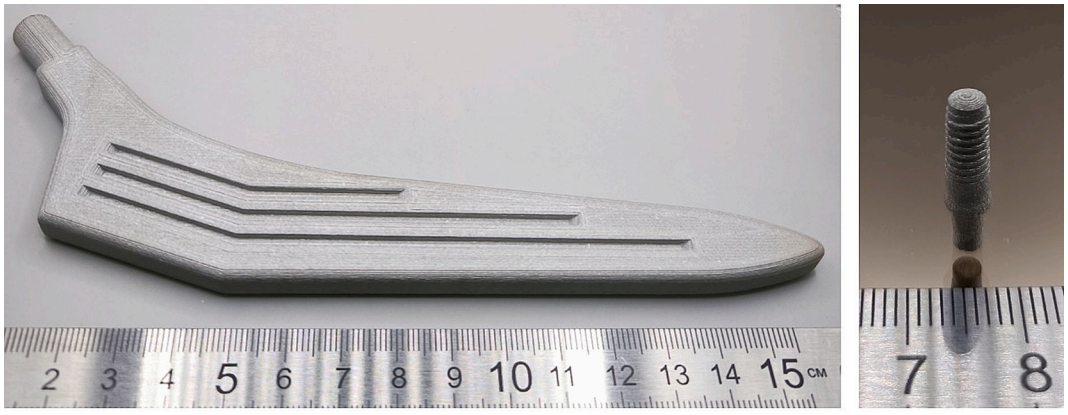

Fig. 7. Printed and sintered (a) hip endoprosthesis and (b) dental implant. The composition of the feedstock was PMMA 40/PEG 45.9/ATBC 14.1 and was produced with kG7E and a blade's rotational speed of 60 rpm during compounding.

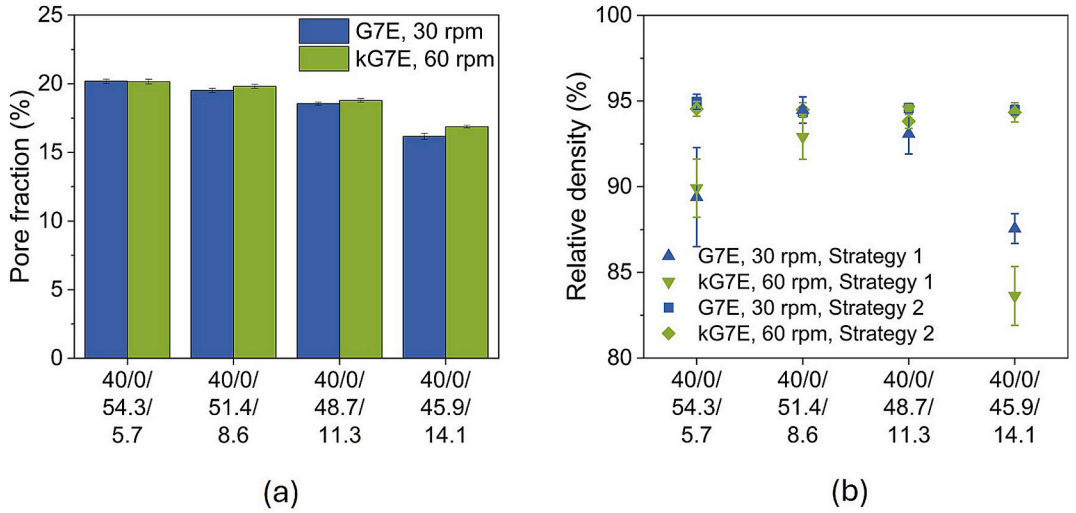

Fig. 8. (a) Pore fraction in samples with different ATBC content after 24 h at 30 °C and (b) relative density of the samples depending on the used thermal debinding and sintering program (PMMA/PVB/PEG/ATBC).

Table 7
Overview of the combinations and parameters investigated.

PMMA/PVB/PEG/ ATBC	Backbone polymers	Time (h)	Rotational speed (rpm)
25/25/44.3/5.7	PMMA G7E, PVB 30H	2	30
25/25/44.3/5.7	PMMA kG7E, PVB 30H	1, 1.5, 2, 3	30
25/25/44.3/5.7	PMMA kG7E, PVB 30H	2	30, 60
22.5/22.5/49.3/5.7	PMMA kG7E, PVB 30H	2	30, 60
20/20/54.3/5.7	PMMA kG7E, PVB 30H	2	30, 60

b). The expelled phase was found to be soluble in water, indicating that the liquid phase consists of PEG. However, it is possible that the substance may also contain parts of the ATBC. Following the compounding process, the feedstocks were extruded into filaments, with the parameters specified in Table 8. The discrepancy in nozzle size is once more process-related and not material-related.

3.3.2. *Rheological characterization*

3.3.2.1. Capillary rheology. The results of the rheological characterization correspond with the compounding behavior and the findings of the separated binder systems. Neither the compounding process (Fig. 10a) nor the compounding time (Fig. 10b) showed any significant effect on the viscosity. An exception is the feedstock which was compounded for three hours. Here, the viscosity is lower, which may be attributed to a more pronounced thermomechanical degradation of the polymer chains. Nevertheless, all feedstocks exhibit a viscosity below 1000 Pas in the printing-relevant shear rate range of 40 to 450 s^{-1}. As previously indicated by the torque during compounding, the partial substitution of PMMA and PVB with PEG resulted in a decrease in viscosity (Fig. 10c). However, binder separation could be observed at high shear rates and with 54.3 vol% PEG, due to reduced entanglement and a decrease in the number of hydrogen bonds between the polymer chains.

3.3.2.2. DMA. In contrast to the flow behavior, the compounding process (Fig. 10d) exhibited a significant impact on the flexibility of the filaments. The use of smaller PMMA pellets and a higher shear rate during the compounding process has resulted in a substantial increase in the flexibility of the filaments. This enhancement is likely attributable to an improved integration of the plasticizer into the feedstock. The same effect was observed for longer compounding times (Fig. 10e). However, extending the mixing time beyond two hours did not result in any additional enhancements. This observation aligns with the torque curve, where the equilibrium phase began after approximately two hours. During this phase, the additive had already been fully integrated into the feedstock, and thus no further improvement in flexibility could be achieved. Fig. 10f shows the impact of the PEG content on the flexibility. As previously referenced in [32], there is a direct correlation between PEG content and flexibility, with higher concentrations resulting in reduced flexibility. This is probably due to the low interaction between ATBC and PEG. Furthermore, similar to the previous observations, a higher shear rate during compounding also led to enhanced flexibility. An exception is again the feedstock produced with 54.3 vol% PEG and a blade's rotational speed of 60 rpm, which exhibited very brittle behavior. This could be attributed to binder separation during the compounding process, where a portion of the ATBC was expelled from the mixing chamber.

3.3.3. *Fused filament fabrication*

The vast majority of filaments, including both stiff and flexible types, demonstrated exceptional printing performance. However, there was an exception observed with the filament produced with 44.3 vol% PEG and a blade's rotational speed of 60 rpm. This filament was ground by the extruder gears due to its low hardness, resulting in the inability to manufacture parts using this feedstock. The printing temperature was dependent on the PEG content; it was 200 °C with 44.3 vol%, 190 °C with 49.3 vol%, and 175 °C with 54.3 vol%. The bed temperature was consistent at 40 °C for all feedstocks. All feedstocks enabled the printing of very delicate parts with a nozzle size of 0.15 mm and very large parts with a nozzle size of 0.8 mm. However, only the two flexible filaments (25/25/44.3/5.7, kG7E, mixing time of 2 or 3 h) offered a high level of usability for printing large parts. The other filaments had to be fed into the extruder as sticks.

3.3.4. *Debinding and sintering*

The combination of PVB and PMMA resulted in pore fractions between the two pure backbone polymers. While the compounding time had no effect on the dissolution of the PEG in water (Fig. 11a), an increase in PEG content led to higher pore fraction after 24 h in water (Fig. 11b). This is likely attributable to the creation of more vast open pores during debinding, which suppresses the blocking effect of the

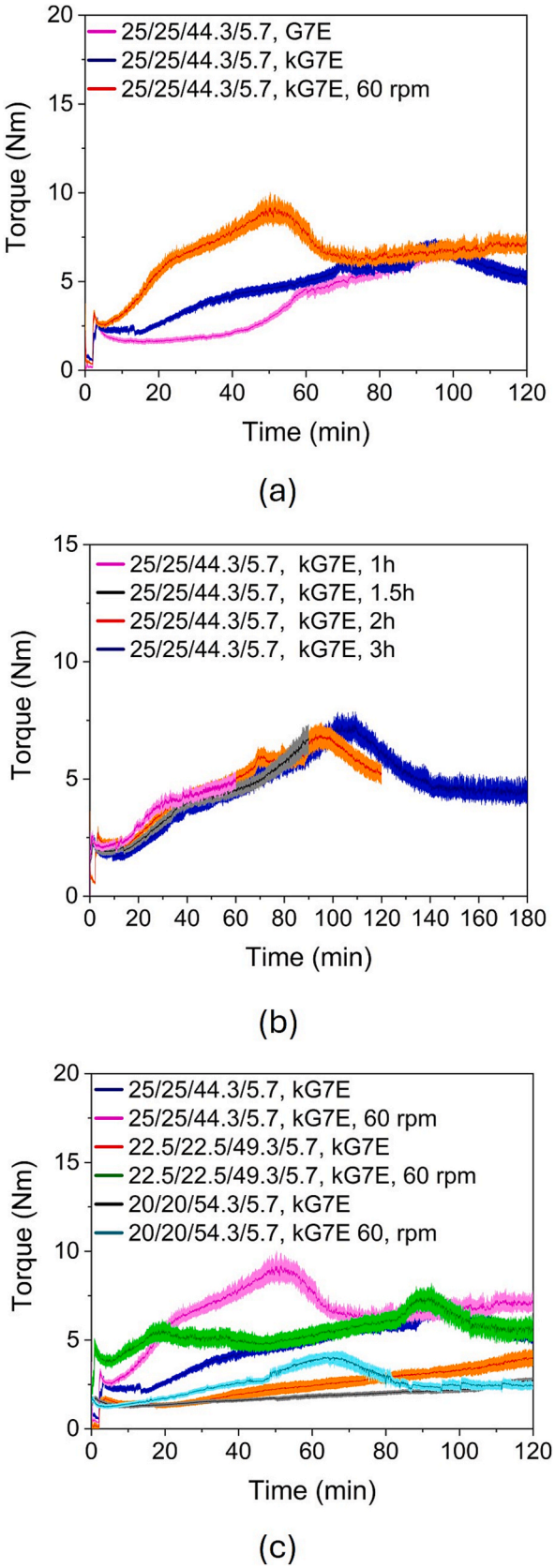

Fig. 9. Compounding of PMMA/PVB/PEG based binder (160 °C) with different compositions and mixing parameters; (a) Variation of PMMA type and blade's rotational speed, (b) variation of compounding time and (c) variation of PEG content and blade's rotational speed (PMMA/PVB/PEG/ATBC).

Table 8
Overview of the extrusion parameters.

PMMA/PVB/PEG/ATBC	PMMA	Flexibility	Temperature (°C)	Nozzle (mm)
25/25/44.3/5.7	G7E	stiff	65	2.7
25/25/44.3/5.7	kG7E	flexible	75	2.95
22.5/22.5/49.3/5.7	kG7E	stiff	65	2.7
20/20/54.3/5.7	kG7E	stiff	65	2.7

backbone polymers. However, an elevated shear rate during compounding resulted in a reduced pore fraction. This phenomenon can be attributed to two possible mechanisms: (1) the separation and expulsion of a portion of the PEG from the mixing chamber during the compounding process, or (2) the increased entanglement of the polymer chains, which reduced the diffusion of the PEG molecules. The densities achieved were contingent upon the debinding strategy employed (Fig. 11c-d). Strategy 1 resulted in poor, characterized by significant variations due to the presence of blisters in the samples. An exception was the feedstock, which was mixed for three hours. In this case, a relative density of 97.7 % was achieved, which may be due to thermal degradation that occurred during the compounding process, thereby enhancing the thermal debinding behavior. In contrast, strategy 2 led to very high relative densities above 98 % for all feedstocks. The samples produced with the feedstock composition PMMA 25/PVB 25/PEG 44.3/ATBC 5.7, a compounding time of 2 h, and a blade's rotational speed of 30 rpm achieved the highest density of 99.5 %. This feedstock has enabled the printing of very delicate parts with complex geometry (Fig. 12a), as well as large parts, such as a femoral stem of a hip endoprosthesis (Fig. 12b). To reduce the stiffness of the implant and enhance cellular proliferation, it is also possible to print the implant with a gyroid structure.

3.4. Elemental analysis

For medical applications, the maximum permissible oxygen and carbon concentrations are 0.2 wt% and 0.08 wt%, respectively [41]. As illustrated in Fig. 13, the remaining carbon and oxygen content in the samples after sintering is dependent on the binder system used. The samples produced with PVB and PEG showed the highest degree of contamination with carbon and oxygen, clearly exceeding the specification, thus contradicting the vendor's assurance of a combustion process without leaving any residues. In addition, the debinding strategy 2, with the pre-debinding process conducted at 250 °C in air, resulted in higher levels of carbon and oxygen. While the increase in oxygen was anticipated, the rise in carbon content was somewhat unexpected. Salam et al. investigated the pyrolysis of PVB in air and an inert atmosphere [61]. Their findings revealed that oxidative degeneration is the sole mechanism capable of achieving complete organic burnout. However, this only occurs within the temperature range of 750–800 °C. At lower temperatures, char is formed, leading to an increase in carbon content. In contrast to PVB, PMMA demonstrated superior debinding behavior. While the carbon content slightly exceeds the standard limit, the oxygen contamination levels meet (strategy 1) or slightly exceed (strategy 2) the specified parameters. These results are consistent with the findings reported in the literature [55,60]. The combination of PMMA and PVB resulted in contaminations that were intermediate between the two pure backbone polymers.

4. Conclusion and Outlook

The study examined the impact of ATBC on various partially water-soluble binder systems, focusing on the flow behavior and the flexibility of the feedstocks as well as the properties of the final components. The results of the study indicated that ATBC can significantly enhance the flexibility of all binder systems, especially those based on PVB. However,

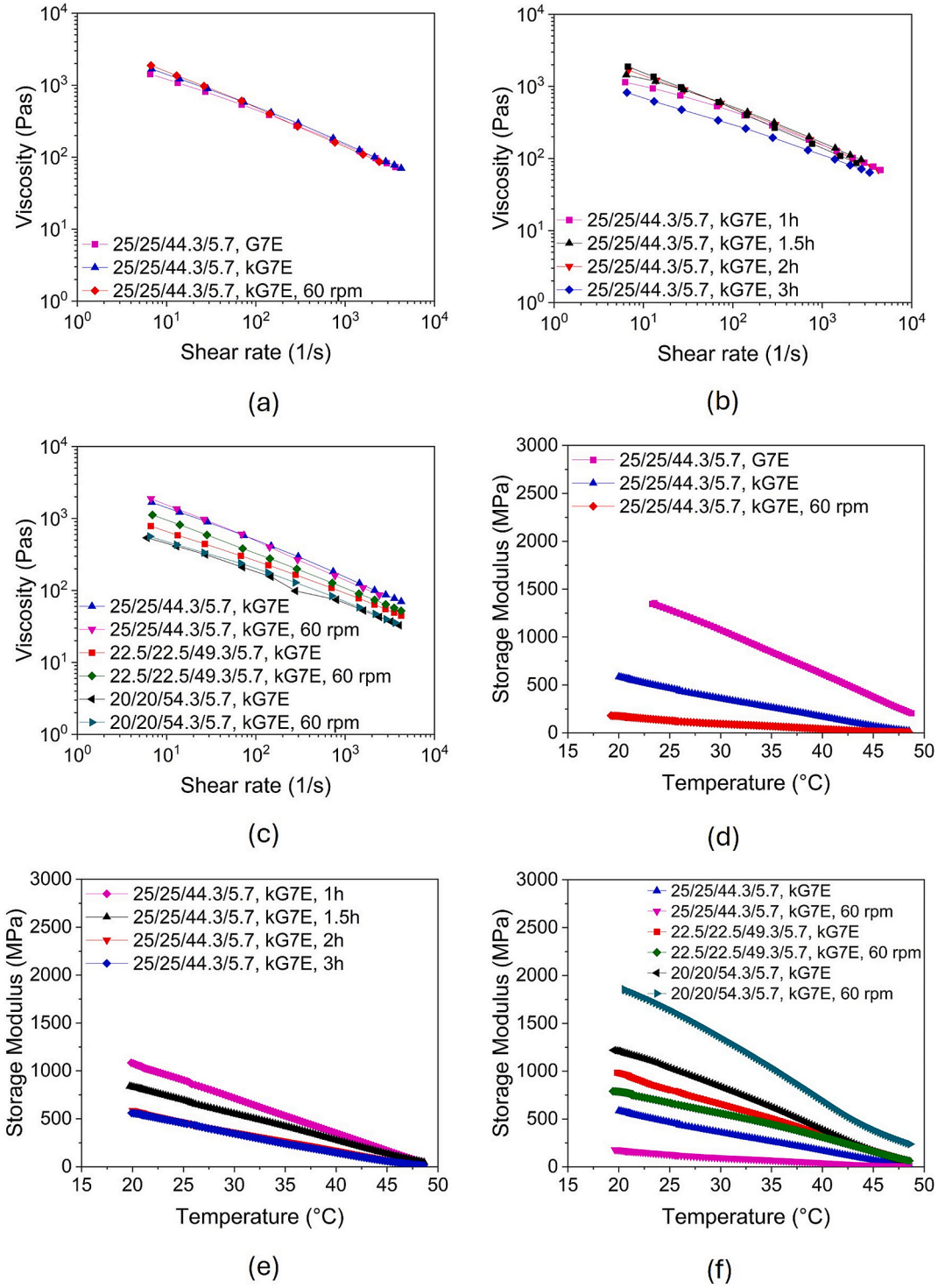

Fig. 10. Capillary rheology of PMMA/PVB/PEG based binder (160 °C) with different compositions and mixing parameters; (a) Variation of PMMA type and blade's rotational speed, (b) variation of compounding time and (c) variation of PEG content and blade's rotational speed. Temperature sweeps of PMMA/PVB/PEG based binder (160 °C) with different compositions and mixing parameters; (d) Variation of PMMA type and blade's rotational speed, (e) variation of compounding time and (f) variation of PEG content and blade's rotational speed (PMMA/PVB/PEG/ATBC).

PVB-based showed an insufficient solvent debinding behavior with deformations of large parts. In this case, PMMA-based feedstocks offer certain advantages, though they result in a lower relative density. The combination of both backbone polymers demonstrated the highest level of usability and superior properties, including excellent flexibility, enabling the printing of complex implants, sufficient green body strength during solvent debinding and high relative densities over 99 %. A challenge that remains is the thermal debinding of feedstocks containing ATBC and PVB. In most cases, debinding in an argon atmosphere has led to defects as well as high carbon and oxygen contents in the samples. Pre-debinding in air could prevent defects, but it has resulted in even more elevated contamination with carbon and oxygen.

Further studies will focus on an improved thermal debinding and sintering process with less contaminations to meet the values in the

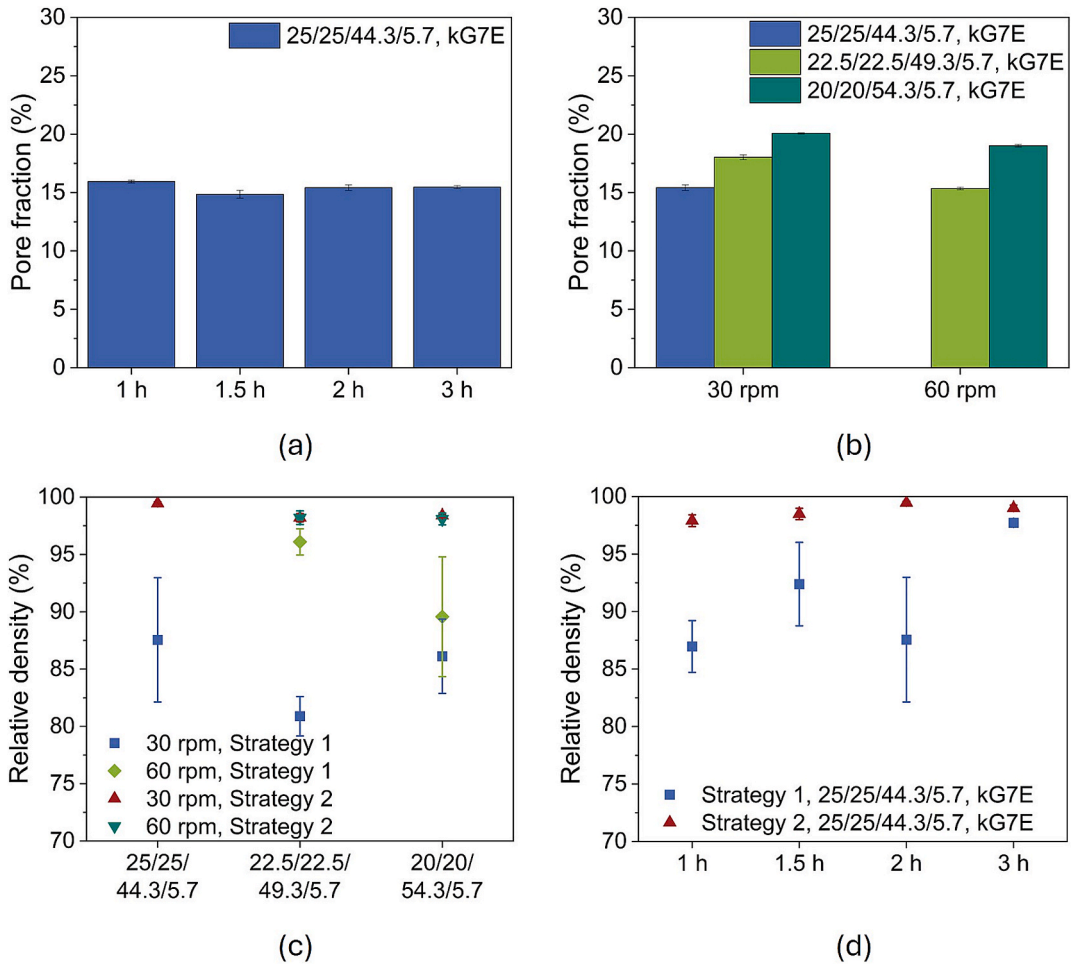

Fig. 11. (a) Pore fraction in samples with different compounding times after 24 h at 30 °C, (b) pore fraction in samples produced with different PEG contents and blade's rotational speed after 24 h at 30 °C, (c) relative density of samples depending on the used thermal debinding and sintering program and (d) relative density of samples depending on the used thermal debinding and sintering program (PMMA/PVB/PEG/ATBC).

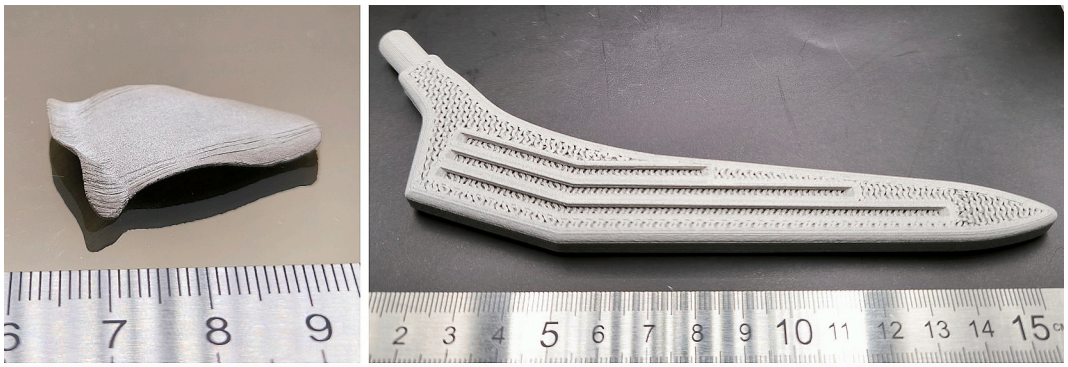

Fig. 12. Printed and sintered (a) skull implant and (b) femoral stem of a hip endoprosthesis with a gyroid structure. The composition of the feedstock was PMMA 25/ PVB 25/ PEG 44.3/ATBC 5.7 and was produced with kG7E.

standard for medical implants. Furthermore, filament driers could expand the range of processible materials with higher PEG content, enhancing the subsequent debinding step. It is also planned that future research will apply the knowledge gained from this study to other fillers, such as ceramics and other metals.

CRediT authorship contribution statement

Ralf Eickhoff: Writing – review & editing, Writing – original draft, Visualization, Validation, Methodology, Investigation, Formal analysis, Conceptualization. **Steffen Antusch:** Writing – review & editing, Validation, Supervision, Methodology. **Dorit Nötzel:** Writing – review & editing, Validation, Supervision, Methodology. **Thomas Hanemann:** Writing – review & editing, Validation, Supervision, Resources, Project

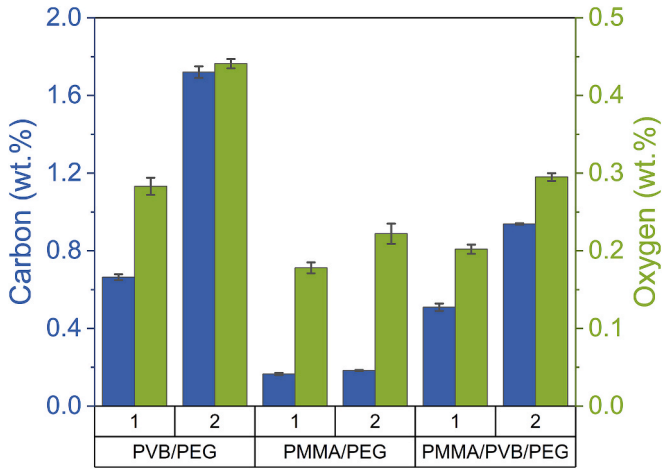

Fig. 13. Elemental analysis after sintering, depending on the binder system and the debinding strategy used.

administration, Funding acquisition.

Funding

This research received no external funding. Open Access funding enabled and organized by Projekt DEAL.

Declaration of competing interest

The authors declare the following financial interests/personal relationships which may be considered as potential competing interests: [Ralf Eickhoff reports financial support, article publishing charges, and equipment, drugs, or supplies were provided by Karlsruhe Institute of Technology. Steffen Antusch reports financial support, article publishing charges, and equipment, drugs, or supplies were provided by Karlsruhe Institute of Technology. Dorit Noetzel reports financial support, article publishing charges, and equipment, drugs, or supplies were provided by Karlsruhe Institute of Technology. Thomas Hanemann reports financial support, article publishing charges, equipment, drugs, or supplies, and travel were provided by Karlsruhe Institute of Technology. Thomas Hanemann reports financial support and equipment, drugs, or supplies were provided by University of Freiburg. If there are other authors, they declare that they have no known competing financial interests or personal relationships that could have appeared to influence the work reported in this paper.].

Acknowledgments

The authors thank the colleagues A. Klein for heat treatment (KIT, Germany), C. Odemer (KIT, Germany) and A. Qazzazie-Hauser (University of Freiburg, Germany) for DSC/TG measurements, M. Raab (KIT, Germany) for powder characterization, and M. Engler and G. Link (KIT, Germany) for providing the DMA.

Appendix A. Supplementary data

Supplementary data to this article can be found online at https://doi.org/10.1016/j.matdes.2025.114088.

References

[1] B. Blakey-Milner, et al., Metal additive manufacturing in aerospace: A review, *Mater. Des.* 209 (12) (2021) 110008, https://doi.org/10.1016/j.matdes.2021.110008.

[2] J.C. Vasco, Chapter 16 - Additive manufacturing for the automotive industry, in: J. Pou, A. Riveiro, J.P. Davim (Eds.), *Additive Manufacturing*, Elsevier, 2021, pp. 505–530.

[3] N. Zhao, et al., Direct additive manufacturing of metal parts for automotive applications, *J. Manuf. Syst.* 68 (2023) 368–375, https://doi.org/10.1016/j.jmsy.2023.04.008.

[4] P. Hanaphy. "Boeing deploys 3D printing to halve the lead time of US Space Force asset." 3D Printing Industry. https://3dprintingindustry.com/news/boeing-deploys-3d-printing-to-halve-the-lead-time-of-us-space-force-asset-205389/ (accessed 28.01., 2025).

[5] M. Salmi, Additive manufacturing processes in medical applications, *Materials (Basel)* 14 (1) (Jan 3 2021), https://doi.org/10.3390/ma14010191.

[6] Y. Zhu, et al., 3D printing biomimetic materials and structures for biomedical applications, *Bio-Des. Manuf.* 4 (2) (2021) 405–428, https://doi.org/10.1007/s42242-020-00117-0.

[7] S. Panda, et al., A focused review on three-dimensional bioprinting technology for artificial organ fabrication, *Biomater. Sci.* 10 (18) (2022) 5054–5080, https://doi.org/10.1039/d2bm00797e.

[8] A.A. Zadpoor, J. Malda, Additive manufacturing of biomaterials, tissues, and organs, *Ann. Biomed. Eng.* 45 (1) (Jan 2017) 1–11, https://doi.org/10.1007/s10439-016-1719-y.

[9] M. Aldesoki, L. Keilig, I. Dorsam, B. Evers-Dietze, T.M. Elshazly, C. Bourauel, Trueness and precision of milled and 3D printed root-analogue implants: A comparative in vitro study, *J. Dent.* 130 (Mar 2023) 104425, https://doi.org/10.1016/j.jdent.2023.104425.

[10] T. Barbin, et al., 3D metal printing in dentistry: An in vitro biomechanical comparative study of two additive manufacturing technologies for full-arch implant-supported prostheses, *J. Mech. Behav. Biomed. Mater.* 108 (Aug 2020) 103821, https://doi.org/10.1016/j.jmbbm.2020.103821.

[11] M. Dehurtevent, L. Robberecht, J.C. Hornez, A. Thuault, E. Deveaux, P. Behin, Stereolithography: A new method for processing dental ceramics by additive computer-aided manufacturing, *Dent. Mater.* 33 (5) (May 2017) 477–485, https://doi.org/10.1016/j.dental.2017.01.018.

[12] L. Zeng, Y. Zhang, Z. Liu, B. Wei, Effects of repeated firing on the marginal accuracy of Co-Cr copings fabricated by selective laser melting, *J. Prosthet. Dent.* 113 (2) (Feb 2015) 135–139, https://doi.org/10.1016/j.prosdent.2014.09.004.

[13] M.Q. Shaikh, et al., "Investigation of patient-specific maxillofacial implant prototype development by metal fused filament fabrication (MF3) of Ti-6Al-4V," (in en), *Dentistry Journal* 9 (10) (2021) 109, https://doi.org/10.3390/dj9100109.

[14] A. Popovich, V. Sufiiarov, I. Polozov, E. Borisov, D. Masaylo, Producing hip implants of titanium alloys by additive manufacturing, *Int. J. Bioprinting* 2 (2) (2024), https://doi.org/10.18063/ijb.2016.02.004.

[15] N.N.A.A. Abdullah, M.I. Ammarullah, Z.F. Mohd Salaha, M.H. Baharuddin, M. R. Abdul Kadir, M.H. Ramlee, Bioinspired porous hip implants design: A systematic review of mechanical testing and additive manufacturing, *Results Eng.* 25 (2025), https://doi.org/10.1016/j.rineng.2024.103708.

[16] C. Song, A. Wang, Z. Wu, Z. Chen, Y. Yang, W. Di, The design and manufacturing of a titanium alloy beak for Grus japonensis using additive manufacturing, *Mater. Des.* 117 (2017) 410–416, https://doi.org/10.1016/j.matdes.2016.11.092.

[17] P. Memarian, et al., Active materials for 3D printing in small animals: current modalities and future directions for orthopedic applications, *Int. J. Mol. Sci.* 23 (3) (Jan 18 2022), https://doi.org/10.3390/ijms23031045.

[18] L.C. Zhang, H. Attar, M. Calin, J. Eckert, Review on manufacture by selective laser melting and properties of titanium based materials for biomedical applications, *Mater. Technol.* 31 (2) (2016) 66–76, https://doi.org/10.1179/1753555715y.0000000076.

[19] J. Kadkhodapour, A. S. Mirhakimi, and H. Montazerian, "Chapter Four - Structural defects and mechanical properties of additively manufactured parts," in *Quality Analysis of Additively Manufactured Metals*, J. Kadkhodapour, S. Schmauder, and F. Sajadi Eds.: Elsevier, 2023, pp. 119-172.

[20] D. Agius, K.I. Kourousis, C. Wallbrink, A review of the as-built SLM Ti-6Al-4V mechanical properties towards achieving fatigue resistant designs, *Metals* 8 (1) (2018), https://doi.org/10.3390/met8010075.

[21] A.K. Singla, et al., Selective laser melting of Ti6Al4V alloy: process parameters, defects and post-treatments, *J. Manuf. Process.* 64 (2021) 161–187, https://doi.org/10.1016/j.jmapro.2021.01.009.

[22] D. Powell, A.E.W. Rennie, L. Geekie, N. Burns, Understanding powder degradation in metal additive manufacturing to allow the upcycling of recycled powders, *J. Clean. Prod.* 268 (2020), https://doi.org/10.1016/j.jclepro.2020.122077.

[23] C. Tosto, J. Tirillò, F. Sarasini, G. Cicala, Hybrid metal/polymer filaments for fused filament fabrication (FFF) to print metal parts, *Appl. Sci.* 11 (4) (2021), https://doi.org/10.3390/app11041444.

[24] Y. Thompson, J. Gonzalez-Gutierrez, C. Kukla, P. Felfer, Fused filament fabrication, debinding and sintering as a low cost additive manufacturing method of 316L stainless steel, *Addit. Manuf.* 30 (2019), https://doi.org/10.1016/j.addma.2019.100861.

[25] R. Eickhoff, S. Antusch, S. Baumgartner, D. Nötzel, T. Hanemann, Feedstock development for material extrusion-based printing of Ti6Al4V parts, *Materials* 15 (18) (Sep 16 2022), https://doi.org/10.3390/ma15186442.

[26] P. Parenti, D. Puccio, Q. Semeraro, B.M. Colosimo, A techno-economic approach for decision-making in metal additive manufacturing: metal extrusion versus single and multiple laser powder bed fusion, *Prog. Addit. Manuf.* (2023), https://doi.org/10.1007/s40964-023-00442-7.

[27] J. Jacob, D. Pejak Simunec, A.E.Z. Kandjani, A. Trinchi, A. Sola, A Review of fused filament fabrication of metal parts (Metal FFF): current developments and future

challenges, *Technologies* 12 (12) (2024), https://doi.org/10.3390/technologies12120267.
[28] J. Abel *et al.*, "Fused Filament Fabrication (FFF) of Metal-Ceramic Components," *J Vis Exp,* no. 143, 2019, doi: 10.3791/57693.
[29] M. Sadaf, M. Bragaglia, F. Nanni, A simple route for additive manufacturing of 316L stainless steel via fused filament fabrication, *J. Manuf. Process.* 67 (2021) 141–150, https://doi.org/10.1016/j.jmapro.2021.04.055.
[30] F. Cerejo, D. Gatões, M.T. Vieira, Optimization of metallic powder filaments for additive manufacturing extrusion (MEX), *Int. J. Adv. Manuf. Technol.* 115 (7–8) (2021) 2449–2464, https://doi.org/10.1007/s00170-021-07043-0.
[31] S. Atre, T. Weaver, and R. and German, "Injection Molding of Metals and Ceramics," 1998.
[32] R. Eickhoff, S. Antusch, D. Nötzel, M. Probst, T. Hanemann, Development of flexible and partly water-soluble binder systems for metal fused filament fabrication (MF3) of Ti-6Al-4V parts, *Polymers* 16 (17) (2024), https://doi.org/10.3390/polym16172548.
[33] G. Wen, P. Cao, B. Gabbitas, D. Zhang, N. Edmonds, Development and design of binder systems for titanium metal injection molding: an overview, *Metall. Mat. Trans. A* 44 (3) (2013) 1530–1547, https://doi.org/10.1007/s11661-012-1485-x.
[34] J. Gonzalez-Gutierrez, S. Cano, S. Schuschnigg, C. Kukla, J. Sapkota, C. Holzer, Additive manufacturing of metallic and ceramic components by the material extrusion of highly-filled polymers: A review and future perspectives, *Materials* 11 (5) (2018), https://doi.org/10.3390/ma11050840.
[35] C. Gloeckle, T. Konkol, O. Jacobs, W. Limberg, T. Ebel, U.A. Handge, Processing of highly filled polymer-metal feedstocks for fused filament fabrication and the production of metallic implants, *Materials* 13 (19) (2020), https://doi.org/10.3390/ma13194413.
[36] Y. Thompson, et al., Fused filament fabrication-based additive manufacturing of commercially pure titanium, *Adv. Eng. Mater.,* 3 (2021) 2100380, https://doi.org/10.1002/adem.202100380.
[37] P. Singh, V.K. Balla, A. Gokce, S.V. Atre, K.H. Kate, Additive manufacturing of Ti-6Al-4V alloy by metal fused filament fabrication (MF3): producing parts comparable to that of metal injection molding, *Prog. Addit. Manuf.* 11 (5) (2021) 840, https://doi.org/10.1007/s40964-021-00167-5.
[38] R.M. German, A. Bose, *Injection molding of metals and ceramics*, Metal Powder Industries Federation, Princeton, N.J., 1997.
[39] M. Chen, et al., Efficient catalytic debinding feedstock design for material extrusion additive manufacturing of low warpage and high-density titanium alloy, *Appl. Mater. Today* 40 (2024), https://doi.org/10.1016/j.apmt.2024.102383.
[40] Z. Lotfizarei, A. Mostafapour, A. Barari, A. Jalili, A.E. Patterson, Overview of debinding methods for parts manufactured using powder material extrusion, *Addit. Manuf.* 61 (2023), https://doi.org/10.1016/j.addma.2022.103335.
[41] *Specification for Metal Injection Molded Titanium-6Aluminum-4Vanadium Components for Surgical Implant Applications*, F. Committee, West Conshohocken, PA, 2023.
[42] T. Ebel, O. Milagres Ferri, W. Limberg, M. Oehring, F. Pyczak, F.P. Schimansky, Metal injection moulding of titanium and titanium-aluminides, KEM 520 (2012) 153–160, https://doi.org/10.4028/www.scientific.net/KEM.520.153.
[43] R. Eickhoff, S. Antusch, D. Nötzel, T. Hanemann, New partially water-soluble feedstocks for additive manufacturing of Ti6Al4V parts by material extrusion, *Materials* 16 (8) (2023) 3162, https://doi.org/10.3390/ma16083162.
[44] R. Heldele, "Entwicklung und Charakterisierung von Formmassen für das Mikropulverspritzgießen," Dissertation, Albert-Ludwigs-Universität Freiburg, Freiburg im Breisgau, 2008.
[45] Y. Gao, K.M. Huang, Z.K. Fan, Z.P. Xie, Injection molding of Zirconia Ceramics using water-soluble binder, KEM 336–338 (2007) 1017–1020, https://doi.org/10.4028/www.scientific.net/KEM.336-338.1017.
[46] N. Chuankrerkkul, P. Sooksaen, P. Pakunthod, T. Kosalwit, W. Pinthong, Powder injection moulding of alumina using PEG/PVB binder systems, KEM 545 (2013) 173–176, https://doi.org/10.4028/www.scientific.net/KEM.545.173.
[47] A.C. Kutlu, D. Nötzel, A. Hofmann, C. Ziebert, H.J. Seifert, I.U. Mohsin, Studies on 3D printing of Na3Zr2Si2PO12 ceramic solid electrolyte through fused filament fabrication, *Electrochim. Acta* 503 (2024), https://doi.org/10.1016/j.electacta.2024.144881.
[48] A. D. Godwin, "Plasticizers," in *Applied Polymer Science: 21st Century*, 2000.
[49] T. Hanemann, R. Heldele, T. Mueller, J. Hausselt, Influence of stearic acid concentration on the processing of ZrO2-containing feedstocks suitable for micropowder injection molding, *Int. J. Appl. Ceram. Technol.* 8 (4) (2011) 865–872, https://doi.org/10.1111/j.1744-7402.2010.02519.x.
[50] J.A. Naranjo, C. Berges, R. Campana, G. Herranz, Rheological and mechanical assessment for formulating hybrid feedstock to be used in MIM & FFF, *Results Eng.* 19 (2023), https://doi.org/10.1016/j.rineng.2023.101258.
[51] N. Venkataraman, et al., Feedstock material property – process relationships in fused deposition of ceramics (FDC), *Rapid Prototyp. J.* 6 (4) (2000) 244–253, https://doi.org/10.1108/13552540010373344.
[52] T. Beran, T. Mulholland, F. Henning, N. Rudolph, T.A. Osswald, Nozzle clogging factors during fused filament fabrication of spherical particle filled polymers, *Addit. Manuf.* 23 (2018) 206–214, https://doi.org/10.1016/j.addma.2018.08.009.
[53] M. Desloir, C. Benoit, A. Bendaoud, P. Alcouffe, C. Carrot, Plasticization of poly (vinyl butyral) by water: glass transition temperature and mechanical properties, *J. Appl. Polym. Sci.* 136 (12) (2018), https://doi.org/10.1002/app.47230.
[54] D. Nötzel, R. Eickhoff, C. Pfeifer, T. Hanemann, Printing of Zirconia parts via fused filament fabrication, *Materials* 14 (19) (2021), https://doi.org/10.3390/ma14195467.
[55] H. Zhang, M.D. Hayat, W. Zhang, H. Singh, K. Hu, P. Cao, Improving an easy-to-debind PEG/PPC/PMMA-based binder, *Polymer* 262 (2022), https://doi.org/10.1016/j.polymer.2022.125465.
[56] G. Chen, P. Cao, G. Wen, N. Edmonds, Debinding behaviour of a water soluble PEG/PMMA binder for Ti metal injection moulding, *Mater. Chem. Phys.* 139 (2–3) (2013) 557–565, https://doi.org/10.1016/j.matchemphys.2013.01.057.
[57] M. Paci, F.P. La Mantia, Competition between degradation and chain extension during processing of reclaimed poly(ethylene terephthalate), *Polym. Degrad. Stab.* 61 (3) (1998) 417–420, https://doi.org/10.1016/s0141-3910(97)00227-9.
[58] M.A. Omar, H.A. Davies, P.F. Messer, B. Ellis, The influence of PMMA content on the properties of 316L stainless steel MIM compact, *J. Mater. Process. Technol.* 113 (1–3) (2001) 477–481, https://doi.org/10.1016/S0924-0136(01)00641-0.
[59] M. D. Hayat, A. Goswami, S. Matthews, T. Li, X. Yuan, and P. Cao, "Modification of PEG/PMMA binder by PVP for titanium metal injection moulding," *Powder Technology,* vol. 315, no. Part A, pp. 243-249, 2017, doi: 10.1016/j.powtec.2017.04.004.
[60] M.D. Hayat, et al., A novel PEG/PMMA based binder composition for void-free metal injection moulding of Ti components, *Powder Technol.* 382 (2021) 431–440, https://doi.org/10.1016/j.powtec.2021.01.009.
[61] L.A. Salam, R.D. Matthews, H. Robertson, Pyrolysis of polyvinyl butyral (PVB) binder in thermoelectric green tapes, *J. Eur. Ceram. Soc.* 20 (9) (2000) 1375–1383, https://doi.org/10.1016/s0955-2219(99)00236-8.